Title

HIGH RESOLUTION POSITRON EMISSION TOMOGRAPHY USING SMALL BISMUTH GERMANATE CRYSTALS AND INDIVIDUAL PHOTOSENSORS

Authors

Derenzo, S.E.
Budinger, T.F.
Vuletich, T.

Publication Date

1982-10-01

LBL-15151
Preprint

Lawrence Berkeley Laboratory

UNIVERSITY OF CALIFORNIA

To be published in IEEE Transactions on Nuclear Science, NS-30(1), 1983.

HIGH RESOLUTION POSITRON EMISSION TOMOGRAPHY USING SMALL BISMUTH GERMANATE CRYSTALS AND INDIVIDUAL PHOTOSENSORS

S. E. Derenzo, T. F. Budinger, and T. Vuletich

October 1982

Biology & Medicine Division

Prepared for the U.S. Department of Energy under Contract DE-AC03-76SF00098

HIGH RESOLUTION POSITRON EMISSION TOMOGRAPHY USING SMALL BISMUTH GERMANATE CRYSTALS AND INDIVIDUAL PHOTOSENSORS*

S.E. Derenzo, T.F. Budinger, and T. Vuletich
Lawrence Berkeley Laboratory and Donner Laboratory
University of California, Berkeley CA 94720

Summary

We describe and compare six detector approaches for coupling small bismuth germanate crystals to individual photosensors.
1) Partial coupling of individual crystals to small cylindrical phototubes.
2) Full coupling of individual crystals to small cylindrical phototubes via shaped lightpipes.
3) Coupling of cylindrical phototubes to individual crystals using three sides of the crystals.
4) Full coupling of individual crystals to small rectangular photomultiplier tubes.
5) Full coupling of groups of crystals to multiple-anode phototubes.
6) Full coupling of groups of crystals to larger rectangular phototubes with either sense wires, solid state photosensors, or UV sensitive wire chambers for crystal identification.

From experimental measurements and Monte Carlo computer simulations we conclude that approaches 5 and 6 are superior in pulse height and timing resolution and are also the best way to read out crystals narrower than 3 mm.

*Supported by D.O.E. Contract DE-AC03-76SF00098 and N.I.H. grant P01 HL25840-03.

1. Introduction

Due to its high density and atomic number, bismuth germanate ($Bi_4Ge_3O_{12}$) can be used in the form of small crystals for high resolution positron emission tomography.[1] However, the low scintillation light yield and the need for good timing and pulse height resolutions make efficient optical coupling to the phototube very important.[2]

This paper presents an analysis of the feasibility and performance of several crystal-phototube coupling schemes suitable for BGO crystals 7 mm or finer. (Figure 1).

2. Coupling of Small BGO Crystals to Individual Phototubes

2.1 Partial Coupling to Cylindrical Phototubes

Figure 1A shows the partial coupling of 5 mm (or 7 mm) crystals to 10 mm (or 14 mm) cylindrical phototubes. Monte-Carlo calculations (using the measured self absorption length of 200 mm) indicate that only 20% of the scintillation light enters the phototube. Using 6 mm x 20 mm x 30 mm deep BGO crystals and 14 mm diameter phototubes (Figure 2), we have measured a pulse height resolution for 511 keV photons of 22% FWHM (full width at half maximum) and a time resolution of 7 nsec FWHM (see Table 1).

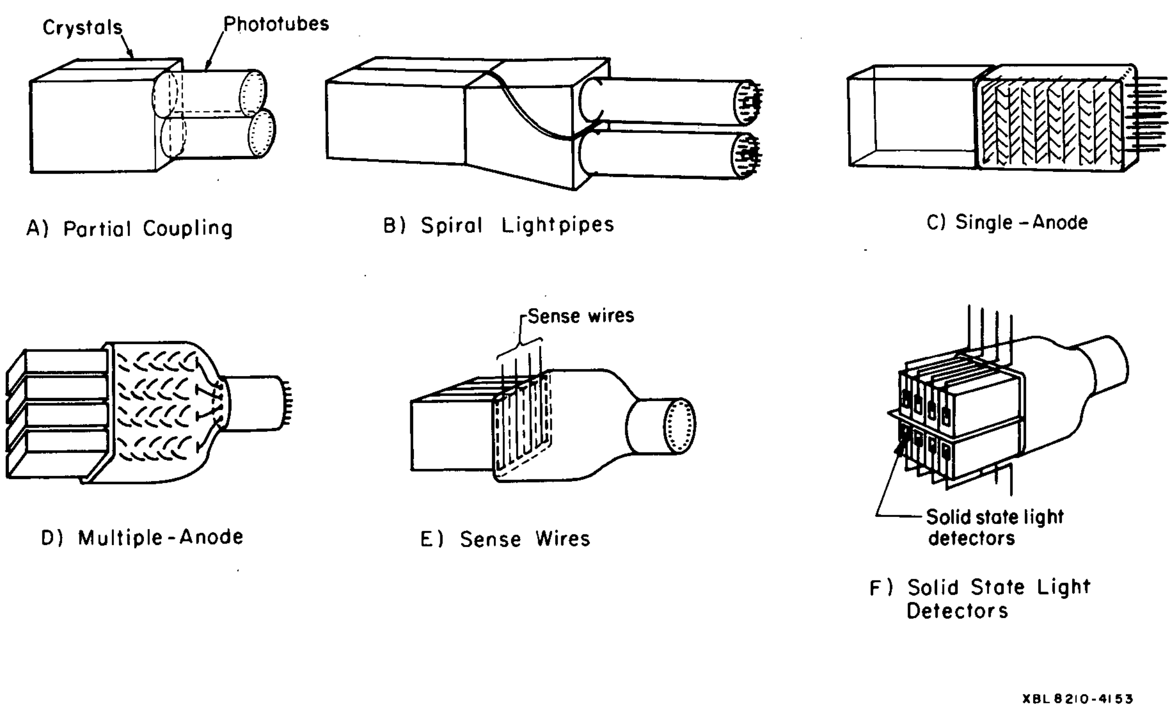

Figure 1: Six schemes for coupling narrow scintillation crystals to individual photodetectors.

2.2 Full Coupling to Cylindrical Phototubes via Lightpipes

Special lightpipes that provide full contact with both the rectangular crystal and the cylindrical phototube were designed and fabricated (Figures 1B and 2). Two close-packed crystals can be coupled to two close-packed phototubes using this lightpipe. This lightpipe has a 14 mm x 14 mm cross section at the phototube end (Figure 3a) and a 6 mm x 20 mm cross section at the end coupled to the BGO crystal (Figure 3e). The pulse height was reduced by a factor of 2.0 relative to scheme 1A and the pulse height resolution was 30% FWHM.

2.3 Coupling to three sides of the Crystal

It is possible to couple 14 mm diameter cylindrical phototubes to crystals as small as 3 mm x 10 mm by using three sides of the crystal. Such a coupling scheme is shown in Figure 4. We have measured a resolution of 18% FWHM for the end coupled detectors and 23% FWHM for the side coupled detectors. The primary disadvantage of this scheme is that it provides only single layer tomography.

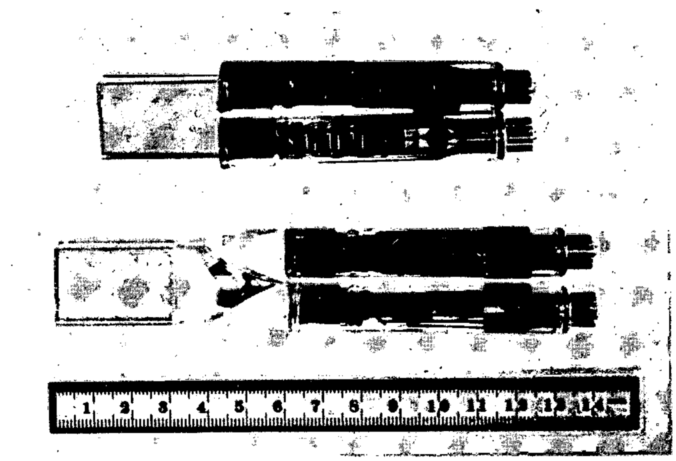

Figure 2: Coupling of BGO crystals with 6 mm x 20 mm faces to 14 mm diameter phototubes. Above- partial contact without lightpipe (Figure 1A). Below- full contact with special lightpipe (Figure 1B).

2.4 Full Coupling to a Small Rectangular Phototube

Recently the development of a 6 mm x 24 mm phototube was announced by Hamamatsu Corp (Figures 1C and 5). The design specifications for quantum efficiency and electron gain are similar to that of their 14 mm cylindrical phototube. The photoelectron yield will then be more than 50% greater than that of scheme 1A with corresponding improvements in timing and pulse height resolution.

3. Multiple-Anode Phototubes

Figure 1D shows direct coupling of a group of crystals to a multiple-anode phototube (Figure 1D). Several such phototubes have been fabricated, including a 24 mm x 24 mm dual tube[3] and a 75 mm x 75 mm quadrant tube.[4] This scheme could, in principle, be used for crystals as fine as 2 mm.

Figure 6 shows a design sketch for an 8-anode phototube for 3 mm x 10 mm crystals based on the electron multiplier geometry used in the rectangular phototube shown in figure 5.

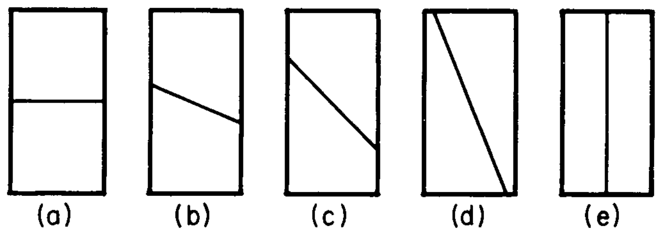

XBL 8210-4166

Figure 3: Cross section of the lightpipe pair shown in the lower portion of Figure 2. The lightpipes have a 14 mm x 14 mm cross section (a) at the end coupled to the phototubes and a 7 mm x 28 mm cross section (e) at the end coupled to the crystals. In the intermediate cross sections (b-d) the boundary between the two lightpipes is a straight line that rotates through 90°.

TABLE 1. COMPARISON OF CRYSTAL-PHOTOTUBE COUPLING ARRANGEMENTS

Figure	1A	1B	1C	1D	1E	1F	4
Minimum crystal width	5 mm	5 mm	6 mm	2 mm	3 mm?	1 mm	~3 mm
photoelectron yield[a]	300	150	450	500	600	600	~350
pulse height resolution (FWHM)	22%	30%	16%[b]	15%[b]	14%	14%	~20%
timing resolution (FWHM)	7 ns	10 ns	6 ns[b]	6 ns[c]	5 ns	5 ns	7 ns

[a]Estimated for a 5 mm wide crystal and 511 keV energy loss
[b]Estimated values
[c]A timing resolution of 2.9 nsec FWHM has been reported for the Hamamatsu R1548, a dual phototube with two 12 mm x 24 mm segments (see Reference 3).

The multi-anode microchannel phototube would be ideal for reading out arrays of small scintillation crystals. The primary requirements for such a device for positron tomography are (i) a long useful lifetime, preferably more than five years of continuous use, and (ii) a very narrow dead zone at the edge of the phototube to permit efficient coupling to a close-packed 2-dimensional array of small crystals. Since the microchannel phototube has excellent timing properties,[5-7] its most important future application may be for time-of-flight positron tomography[8-11] with high spatial resolution.

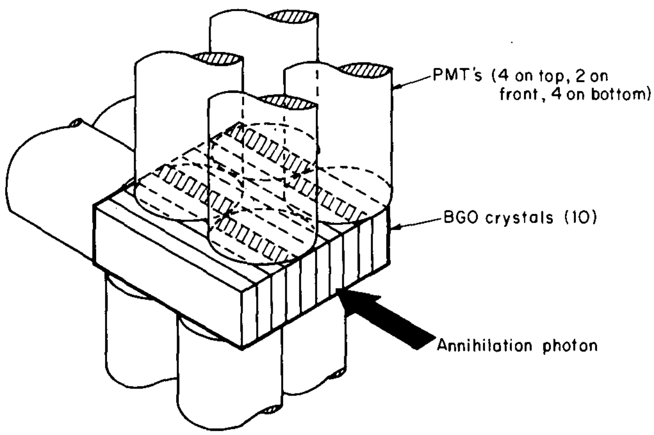

Figure 4: Scheme for coupling 3 mm x 10 mm BGO crystals to individual 14 mm phototubes. Only the cross-hatched area of each crystal is coupled to the corresponding phototube. This design can be used only for a single ring.

4. Crystal Identifiers

In this approach a group of crystals is directly coupled to a larger phototube which provides timing and pulse height information. The identity of the crystal producing the scintillation light is determined by special crystal identification schemes discussed below. The major disadvantage is the inability to handle two detections in a crystal group within a short period of time and this limits the maximum event rate.

4.1 Sense Wires

In this scheme sense wires are used to control the photocathode emission and identify the crystal producing the scintillation light (Figure 1E). This idea was developed by Charpak[12,13] and also investigated by Boutot.[14] A series of very brief pulses is applied sequentially to wires under each crystal. When the wires under a scintillating crystal are energized, the photoelectron current is briefly interrupted and this can be detected by its effect on the shape of the anode pulse.

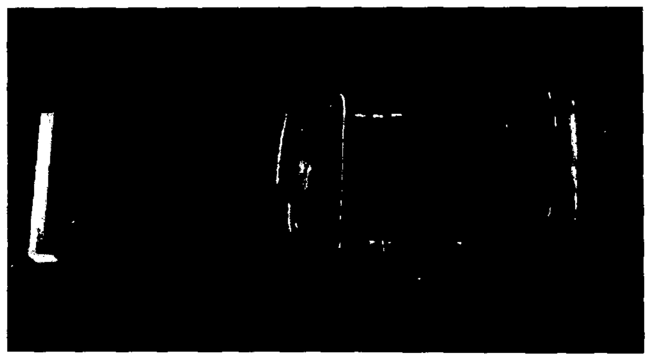

Figure 5: BGO crystal with 6 mm x 20 mm face coupled to a small rectangular phototube being developed by Hamamatsu Corp. of Japan. Unit in this photograph is a non-operating mechanical sample.

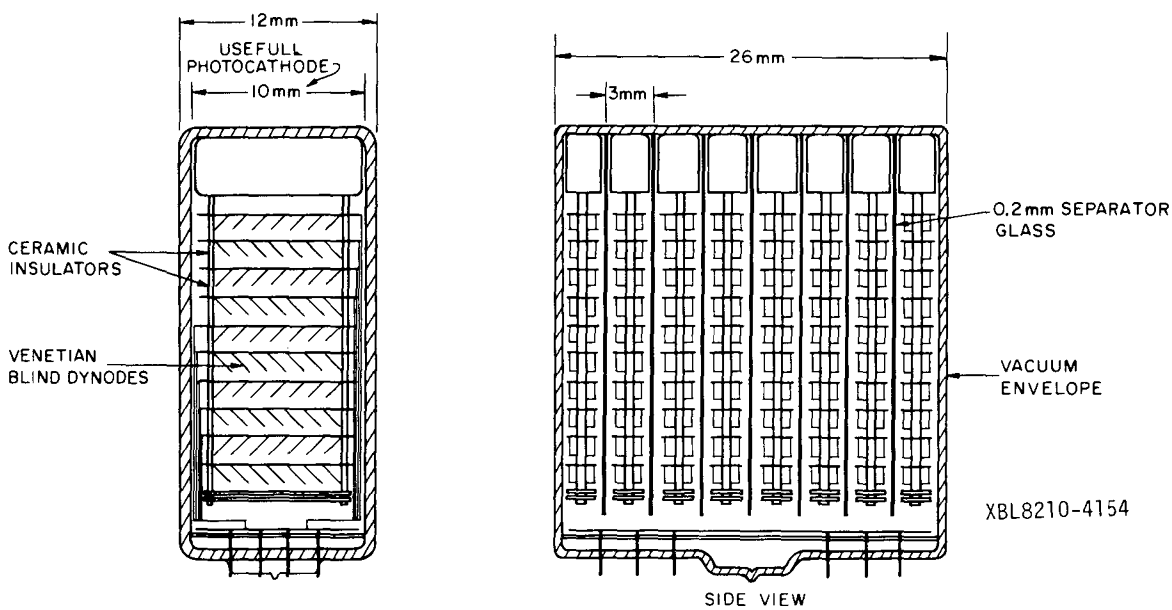

Figure 6: Sketch of eight-anode phototube for reading out a group of eight 3 mm x 10 mm crystals.

TABLE 2. Monte Carlo Calculation of Light Collected by a Photomultiplier and a HgI_2 Photosensor Coupled to the Same BGO Crystal[a].

HgI_2 Coupling Fraction	0.0	0.1	0.2	0.5	1.0
Phototube Coupling Fraction	1.0	1.0	1.0	1.0	1.0
CASE I: HgI_2 Crystal Glued to BGO Crystal (assumed index of refraction of glue 1.52)					
Collected by HgI_2	0%	2.1%	4.0%	10%	20%
Collected by Phototube	37%	34%	33%	28%	20%
Absorbed by External Reflectors	15%	14%	14%	14%	13%
Absorbed in Crystal	48%	49%	48%	48%	47%
CASE II: HgI_2 Crystal Grown Directly on BGO Crystal (assumed index of refraction of HgI_2 3.00)					
Collected by HgI_2	0%	11%	19%	37%	55%
Collected by Phototube	36%	33%	30%	23%	16%
Absorbed by External Reflectors	14%	14%	13%	12%	10%
Absorbed in Crystal	50%	43%	38%	29%	19%

[a]Absorption length 40 cm, Bubble interaction length 40 cm. Diffuse external reflectivity 98%, 10,000 scintillation photons per run.

4.2 Solid State Photodetectors

A second method for crystal identification uses solid state photosensors for the identification of the scintillating crystal, as shown in Figure 1F and discussed in the following sub-sections. It is desired that the solid state photosensor have sufficient pulse height resolution to reject events where a significant amount of energy (e.g. >100 keV) has been lost in more than one crystal. It is also important that a large fraction of one crystal face be coupled to the photosensor. Table 2 shows results of a Monte Carlo analysis of the dependence of pulse height on coupling fraction. One disadvantage of solid state photosensors is that their quantum efficiency falls off sharply for wavelengths shorter than 400 nm. They are very efficient for BGO (480 nm) but very inefficient for BaF_2 (225 and 310 nm).

4.2.1 Silicon Photodiodes: The scintillation light from a 511 keV annihilation photon in a BGO crystal makes 1800 electron-hole pairs (0.28 fC) in the photodiode. This small signal requires amplification by a state-of-the-art charge amplifier with a low-noise FET input stage. Small, inexpensive amplifiers of this type have been developed by several groups.[15,16]

Conventional silicon photodiodes have a capacitance of approximately 10 pF per mm^2 and this leads to a typical noise broadening of 0.4 fC FWHM (see Appendix). This capacitance can be reduced by a factor of 2-3 by the application of a back-bias of several volts, but the resulting current produces a shot noise that results in an overall increase in noise.

Recently Cavalli[17] using specially fabricated silicon photodiodes (Hamamatsu Corp.) with low bias current (1-10 nA) and low capacitance (70 pF for 100 mm^2) has reported an rms noise level of 200 keV when observing pulses from 662 keV gamma rays. This is a substantial advance, but insufficient for the reliable detection of 511 keV photons.

4.2.2 Silicon Avalanche Photodiodes: For several years it has been known that a back-biased silicon photodiode can exhibit an electron avalanche gain of 100. In principle, since this amplification occurs before the preamplifier, the signal-to-noise ratio should be improved. However, such devices have been plagued by non-uniformity, were very small (only a few mm^2) and very expensive. In spite of these limitations, several years ago G. Huth was able to detect a photopeak from 511 keV photons on BGO.

Recently, Entine et al of Radiation Monitoring Devices Inc. have developed a new fabrication technique that produces very uniform (gain variations <7%) avalanche photodiodes as large as 1 cm^2.[18] They report a pulse height resolution of 9.5% FWHM for 662 keV gamma rays on NaI(Tl). Since the quantum efficiency of silicon is higher for BGO than for the bluer light of NaI(Tl), we expect that this result is equivalent to 20% FWHM for annihilation photons on BGO. Unfortunately, these devices are still in the experimental stage and are very expensive ($10,000 per device). RCA, Inc. also is developing avalanche photodiodes for the same purpose.[19] It is expected that large scale fabrication could bring about a significant reduction in cost.

4.2.3 HgI_2 Photodetectors: Recent work by Iwanczyk et al demonstrates that HgI_2 can detect the 480 nm scintillation light from BGO with a quantum efficiency of about 70%.[20] HgI_2 has a large band gap (2.2 eV) and low leakage current (<1 nA) even when used with a high bias voltage. Moreover, the capacity is approximately 1 pF per mm^2, 10 times less than that of conventional silicon photodiodes. These workers have measured a pulse height resolution of 19% for 511 keV annihilation photons on BGO using low noise charge amplifiers developed by them for ultralow-energy X-ray detection.[16,21] The electronic noise of their charge amplifier was 0.04 fC (pulse peaking time 8 μsec) and the 511 keV photon signal was 0.28 fC (1750 electron-hole pairs). Thus we expect a resolution broadening of 13% from electronic noise and 6% from electron-hole statistics. Other sources of resolution degradation are discussed in their paper.[20]

The application of this approach to high resolution Positron Tomography is also being investigated by Barton et al.[22]

A Monte Carlo computer code developed for simulating the fate of photons in scintillators[2] was used to calculate the percentage of light entering the photomultiplier and the solid state photosensor (Figure 1F). The results (Table 2) show that a large coupling fraction is necessary for efficient light collection and that if the HgI_2 crystal could be grown directly on the BGO crystal, then the light transferred to the HgI_2 would increase by more than a factor of three with only a slight reduction in the light entering the phototube.

4.3 Imaging Proportional Chamber

Recent work by Charpak,[23] Anderson,[24,25] Ku,[26] and by Sauli[27] has resulted in the development of a multiwire proportional chamber with a filling gas having a low enough ionization potential to detect UV emissions from a xenon gas scintillator. This approach works quite well for imaging X-rays because the xenon gas has high detection efficiency and produces UV photons of 8 eV, which the imaging proportional chamber can easily detect. The primary disadvantage for the detection of 511 keV annihilation photons is that it can only be used with scintillators that produce photons of energy 5.3 eV or greater.

One application of the imaging proportional chamber is in the identification of scintillating BaF_2 crystals which are viewed by a large, high speed phototube with a UV transmitting window. This would improve the spatial resolution of BaF_2 time-of-flight systems.

It would be desirable to find a scintillator with a detection efficiency comparable to BGO that produces UV light suitable for detection by these multiwire proportional chambers.

5. Conclusions

The use of conventional cylindrical phototubes with special packing schemes and lightpipes does not provide efficient optical coupling, especially for small crystals.

The use of groups of crystals coupled to larger phototubes and solid-state photosensors to identify the scintillating crystal provides more efficient coupling and better timing and pulse height resolutions. However, maximum rates will be limited by the inability of this approach to handle two detections in a crystal group within a short period of time. Both the silicon avalanche photodiode and the HgI_2 photosensor have sufficient signal-to-noise ratio to reliably identify scintillating crystals and even reject multiple-crystal interactions. The light collection by HgI_2 can be tripled by growing the HgI_2 crystal directly onto the BGO crystal rather than using conventional coupling media.

The best approach considered here requires the development of a multi-anode phototube for small crystals. This provides efficient coupling, can handle small crystals in parallel at high rates, and does not require auxiliary photosensors and associated electronics.

APPENDIX

Noise in Charge Amplifiers as a Function of Photosensor Capacitance

The noise in charge amplifiers is a function of the parameters of the FET, the capacitance and bias current of the photodetector, the Johnson noise of the feedback resistor, and the pulse shaping time constants. From equation 24 of Reference 28, the primary noise component is the delta noise from the FET input stage. For RC pulse shaping with equal RC integration and differentiation times t_o, the resolution broadening is given by:

$$\sigma^2(\text{rms electrons}) = \frac{0.5\ kTC^2e^2}{q^2 g_m t_o} \qquad (1)$$

where k is the Boltzmann factor (1.374×10^{-23} Joule/°K), T is the temperature, C is the total capacitance, e is the base of the natural logarithms, q is the charge of the electron (1.6022×10^{-19} Coul), and q_m is the transconductance of the FET. At 300°K this reduces to:

$$\Gamma(\text{FWHM Coul}) = \frac{2.90 \times 10^{-10}\ C}{\sqrt{g_m t_o}} \qquad (2)$$

For the 2N4391 FET with a g_m of 20mA/V and t_o = 5 μsec, eqn (2) reduces to Γ = 0.92 μV•C. The internal capacitance is about 15 pF.

We have measured the noise levels in a typical charge amplifier for load capacitances from 0 pF to 270 pF and find that for t_o = 5 μsec, the noise is accurately described by:

$$\Gamma(\text{FWHM Coul}) = 1.4\ \mu V \cdot (45\ pF + C_L) \qquad (3)$$

This is somewhat larger than the expected value from equation (2) due to other noise sources.

Using t_o = 1 μsec we find:

$$\Gamma(\text{FWHM Coul}) = 2.1\ \mu V \cdot (35\ pF + C_L) \qquad (4)$$

Since the capacitance of an unbiased 30 mm^2 silicon photodiode is typically 300 pF, the noise level is approximately 0.4 fC FWHM, 1.5 times larger than the signal. The application of a back-bias will reduce the capacitance, but the resulting bias current I introduces a noise term given by:

$$\Gamma(\text{FWHM Coul}) = \sqrt{I\ t_o q} \qquad (5)$$

For t_o=5μsec, a current of only 100 nA results in a FWHM of 0.28 fC, which is equal to the 511 keV signal.

On the other hand, a biased 30 mm^2 HgI_2 detector has <1 nA current, only 30 pF capacitance and can be used with a low capacity FET. The resulting noise level is ~0.03 fC, ten times smaller than the 511 keV signal.

Acknowledgments

We thank J. Cahoon, R. Huesman and D. Landis for helpful discussions, J. Riles for programming assistance, M. Cavalli, D. Coyne, and D. Groom for preliminary data on low-noise silicon photodiodes, A. Dabrowski and J. Iwanczyk for preliminary data on HgI_2 photosensors, and R. Stevens for drafting. This work was supported by the Office of Health and Environmental Research of the U.S. Department of Energy under Contract No. DE-AC03-76SF00098 and also by the National Institutes of Health, National Heart, Lung, and Blood Institute under grant No. P01 HL25840-03.

REFERENCES

1. Derenzo SE: Monte Carlo calculations of the detection efficiency of arrays of NaI(Tl), BGO, CsF, Ge, and plastic detectors for 511 keV photons. IEEE Trans Nucl Sci NS-28: No 1, 131-136, 1981

2. Derenzo SE and Riles J: Monte Carlo calculations of the optical coupling between bismuth germanate crystals and photomultiplier tubes. IEEE Trans Nucl Sci NS-29: No 1, 191-195, 1982

3. Yamashita T, Ito M, and Hayashi T: New dual rectangular photomultiplier tube for positron CT. Proceedings of the International Workshop on Physics and Engineering in Medical Imaging, Asilomar, CA, March 15-18, 1982

4. Persyk DE, Morales J, McKeighen R, et al: The quadrant photomultiplier. IEEE Trans Nucl Sci NS-26: No 1, 364-367, 1979

5. Bateman JE, Apsimon RJ and Barlow FE: A new photomultiplier tube utilising channel plate electron multipliers as the gain producing elements. Nucl Instr Meth 137: 61-70, 1976

6. Lo CC, Leskovar B: Performance studies of high gain photomultiplier having Z-configuration microchannel plates. IEEE Trans Nucl Sci NS-28: No 1, 698-704, 1981

7. Nieschmidt EB, Lawrence RS, Gentillon CD, et al: Count rate performance of a microchannel plate photomultiplier. IEEE Trans Nucl Sci NS-29: No 1, 196-199, 1982

8. Allemand R, Gresset C, and Vacher J: Potential advantages of a Cesium Fluoride scintillator for a time-of-flight positron camera. J Nucl Med 21: 153-155, 1980

9. Mullani NA, Ficke DC, and Ter-Pogossian MM: Cesium Fluoride: a new detector for positron emission tomography. IEEE Trans Nucl Sci NS-27: No 1, 572-575, 1980

10. Ter-Pogossian MM, Mullani NA, Ficke DC, et al: Photon time-of-flight-assisted positron emission tomography. J Comput Assist Tomogr 5: 227-239, 1981

11. Gariod R, Allemand R, Cormoreche E, and Laval M: The "LETI" positron tomograph architecture and time of flight improvements. Proceedings of the Workshop on Time-of-Flight Tomography, Washington University, St. Louis MO, May, 1982

12. Charpak G: The localization of the position of light impact on the photocathode of a photomultiplier. Nucl Instr Meth 48: 151-153, 1967

13. Charpak G: Retardation effects due to the localized application of electric fields on the photocathode of a photomultiplier. Nucl Instr Meth 51: 125-128, 1967

14. Boutot JP and Pietri G: Photomultiplier control by a clamping cross-bar grid. IEEE Trans Nucl Sci NS-19: No 3, 101-106, 1972

15. Landis DA, Adachi RS, Madden NW, et al: Low noise preamplifiers/amplifiers for the time projection chamber . IEEE Trans Nucl Sci NS-29: No 1, 573-577, 1982

16. Dabrowski AJ, Iwanczyk JS, Barton JB, et al: Performance of room temperature mercuric iodide (HgI_2) detectors in the ultra-low energy region. IEEE Trans Nucl Sci NS-28: No 1, 536-540, 1981

17. M. Cavalli, Princeton University, private communication, 1982

18. Entine E, Serreze HB, Reiff G, et al: Scintillation detectors using large area silicon avalanche photodiodes. IEEE Trans Nucl Sci NS-30: No 1, 1983

19. Capasso F: Avalanche photo diodes with enhanced ionization rates ratio: towards a solid state photomultiplier. IEEE Trans Nucl Sci NS-30: No 1, 1983

20. Iwanczyk J, Barton J, Dabrowski J, et al: A novel radiation detector consisting of an HgI_2 photodetector coupled to a scintillator. IEEE Trans Nucl Sci NS-30: No 1, 1983

21. Iwanczyk JS, Kusmiss JH, Dabrowski AJ, et al: Room-temperature mercuric iodide spectrometry for low-energy X-rays. Nucl Instr Meth 193: 73-77, 1982

22. Barton J, Hoffman E, Iwanczyk J, et al: High-resolution detection system for positron tomography. IEEE Trans Nucl Sci NS-30: No 1, 1983

23. Charpak G, Policarpo A, and Sauli F: The photoionization proportional scintillation chamber. IEEE Trans Nucl Sci NS-27: No 1, 212-215, 1980

24. Anderson DF: A xenon gas scintillation proportional counter coupled to a photoionization detector. Nucl Instr Meth 178: 125-130, 1980

25. Anderson DF: A photoionization detector for the detection of xenon light. IEEE Trans Nucl Sci NS-28: No 1, 842-848, 1981

26. Ku WH and Hailey CJ: Properties of an imaging gas scintillation proportional counter. IEEE Trans Nucl Sci NS-28: No 1, 830-839, 1981

27. Sauli F: The gas photodiode as a possible large area photon detector. IEEE Trans Nucl Sci NS-30: No 1, 1983

28. Goulding FS and Landis DA: Semiconductor detector spectrometer electronics. In Nuclear Spectroscopy and Reactions, part A, Academic Press, New York, 1974 pp 413-468